XL CILAMCE
IBERO-LATIN AMERICAN CONGRESS ON COMPUTATIONAL METHODS IN ENGINEERING
NOVEMBER 11-14, 2019
Praiamar Natal Hotel & Convention
Natal, RN-BRAZIL

DEVELOPMENT OF A FINITE ELEMENT MODEL OF STEEL-CONCRETE COMPOSITE ALVEOLAR BEAMS

Matheus E. Benincá
Inácio B. Morsch
matheuseb@hotmail.com
morsch@ufrgs.br
Programa de Pós-Graduação em Engenharia Civil - UFRGS
Av. Osvaldo Aranha, 99, 90035-190, Porto Alegre, RS, Brasil

Abstract. The use of steel-concrete composite beams allows the best properties of these materials to be explored, enabling the design of larger spans and the achievement of more economical structural solutions. The alveolar steel beams, in turn, provide a greater rationalization in the use of this material, since, with almost the same amount of steel, expanded profiles are produced with greater moment of inertia and, consequently, greater flexural strength and better performance under serviceability limit states. Through the union of these structural systems the composite alveolar beams are obtained, in which the advantages of the two systems are enhanced, and their disadvantages are mitigated. Thus, it is possible to reduce materials consumption and, consequently, the generation of environmental impacts. Considering that the Brazilian and the international standards do not specify criteria for analysis and design of composite alveolar beams, numerical and experimental studies have been carried out at the academic level in order to deepen the understanding about the behavior of these structures, whose complexity involves the occurrence of different modes of collapse. The present work aims to contribute to the advances in the field of numerical analysis of composite alveolar beams by developing a finite element model with ANSYS software, version 19.2, in which the steel profile was modeled by shell elements, the concrete slab by hexahedral solid elements, the connectors by non-linear spring elements, the steel deck sheet by shell elements and the slab reinforcement bars by embedded elements. In order to capture the effects of local instabilities, initial geometric imperfections were added to the profile through the combination of buckling modes. For the simulation of concrete behavior, two models have been used: the first, denominated DP-Concrete, is a native ANSYS model, available in the more recent versions of this software; and the second, denominated usermat, is a customizable model based on Ottosen criterion. The validation of the model was done through the numerical analysis of beams tested experimentally by other authors. The obtained results presented a good correlation with the experimental results and with numerical results from previous works.

Keywords: Finite Element Method, Composite Beams, Cellular Beams, Castellated Beams.

1 Introduction

The use of steel-concrete composite beams has been widespread in the civil construction sector, as it allows the best mechanical properties of the involved materials to be explored. In these beams, a steel profile is connected to a concrete slab through shear connectors, which aim to restrict longitudinal slip and vertical separation at the interface [1], ensuring the joint work of the materials. This configuration allows to use these materials more rationally, especially in beams that are simply supported, where the concrete basically works under compression and the steel profile under tension. The result of this rationalization is an increase in the strength of the composite beam, when compared to the materials working separately, which allows the projects of larger spans and/or the achievement of more economical structural solutions [2].

Another possible solution to overcome large spans and rationalize construction is the use of steel alveolar beams, which consist of steel profiles with sequential openings in the web. The great advantage of this type of beam is a result of its manufacturing process: the original steel profile is cut longitudinally in a certain pattern so that the two resulting halves can be repositioned and then welded together in a new configuration, in which the flanges are farther apart, as shown in Fig. 1. That is, with practically the same weight and volume of steel a new profile is manufactured with higher height, and consequently greater moment of inertia and resistance to bending. According to the shape of the holes, generally known as alveoli, these beams can be called as *castellated beams*, when their holes have a hexagonal shape; or as *cellular beams*, when they are circular in shape.

Figure 1. Manufacturing process of castellated beams [3].

Although the use of alveolar beams has many advantages, such as increased flexural strength, better performance under serviceability limit states, the possibility of passage of pipes through the alveoli and optimization of the ceiling height in buildings, among others, these beams also have a significant disadvantage, that is the reduction in shear strength compared to full web beams. Consequently, they are inefficient in resisting the stresses of concentrated loads, often requiring reinforcements on the web, thus increasing their cost [4], [5].

Moreover, due to the peculiarity of their geometry and consequently of their structural behavior, the alveolar beams have specific modes of collapse, which must be properly understood, aiming at their correct use as a structural element. Kerdal and Nethercot [6] studied these failure modes, which are: (i) Formation of a Vierendeel mechanism; (ii) Buckling of web post due to shear; (iii) Rupture of a welded joint in a web post; (iv) Lateral-torsional buckling of an entire span; (v) Formation of a flexure mechanism (hinge); and (vi) Buckling of web post due to compression.

In order to maximize advantages, mitigate disadvantages and further rationalize the use of the materials involved, it is possible to unite the two structural systems discussed so far, through the utilization of composite beams of concrete and alveolar steel profiles, called as *composite alveolar beams*. This union has been the target of academic research in the last decades and has been widespread and used in civil construction, as it enables the reduction of materials consumption and, consequently, leads to more economical solutions and less environmental impacts. Figure 2 illustrates ArcelorMittal's Global Research & Development Centre [7], with composite cellular beams on the roof, utilizing the steel-deck system.

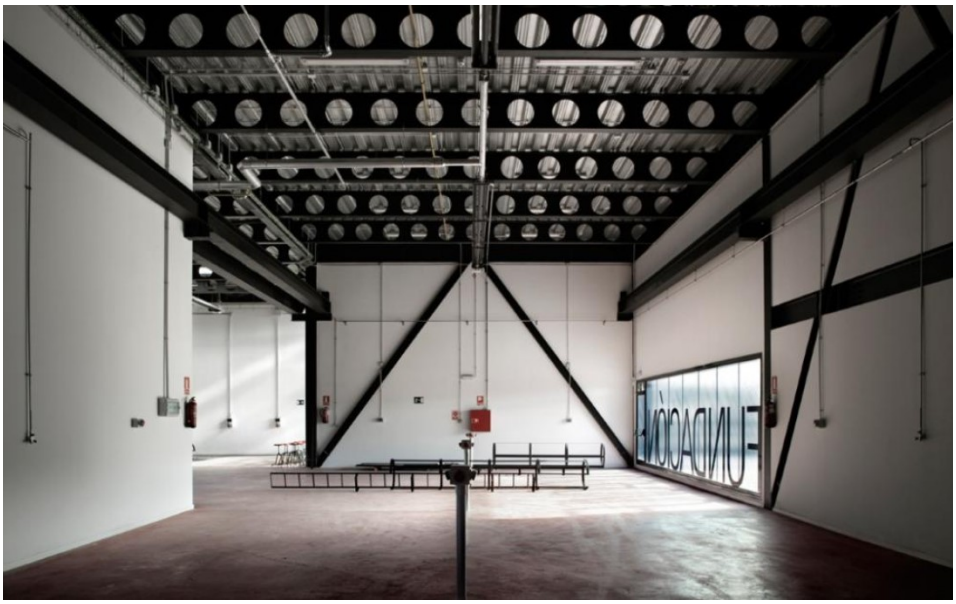

Figure 2. ArcelorMittal's Global Research & Development Centre [7].

According to Badke-Neto, Calenzani and Ferreira [5], due to the increased stiffness of the alveolar beam compared to the full web beam, the composite alveolar beams can overcome even larger spans than the traditional composite beams. Likewise, the concrete slab's contribution of stiffness enables them to overcome larger spans and resist higher loads than alveolar beams working isolatedly.

However, according to Gonçalves [3], the presence of the concrete slab influences the failure modes of the alveolar beam, modifying them and even creating the possibility of new modes. It is essential that this differentiated behavior is properly studied and understood in order to be properly considered in structural calculation. Brazilian and international standards approach composite steel and concrete structures, but do not specify criteria for the calculation of composite alveolar beams.

In this context, the goal of the present work is to develop a finite element model for the numerical simulation of composite alveolar beams, aiming to create a tool that helps understanding the behavior of these structures. The developed model will be validated by comparing its results with experimental results from the tests made by Nadjai et al. [8].

2 Numerical model

The numerical model was developed in ANSYS software, version 19.2. In this section, the element types, material models, boundary conditions and solution stages are presented.

2.1 Element types

The concrete slab was modeled by hexahedral elements with twenty nodes and three degrees of freedom per node (translations in x, y and z), called SOLID186 in ANSYS [9]. In the present work these elements were used in their homogeneous form with full integration. Its formulation is based on Zienkiewicz [10]. Because it is a current-technology element, SOLID186 is compatible with several current ANSYS features, such as the generation of embedded elements and the use of new material models, e.g. DP-Concrete.

The reinforcement bars were modeled by discrete embedded elements, called REINF264 in ANSYS [9], which are suitable for simulating steel bars. These elements use the same nodes of the base elements SOLID186, even if their geometric position does not coincide with them. The REINF264 element presents only axial stiffness, thus the stiffnesses to bending, torsion and shear stress are neglected. A perfect interaction between the reinforcing element and the concrete base element is

admitted, so there is no relative movement between them [9].

For the generation of reinforcement embedded elements, a new ANSYS functionality was used, denominated mesh-independent method. This method uses MESH200 elements, which are only guide elements, and thus do not directly contribute to the solution, but determine the positions where REINF264 reinforcement elements are created. Therefore, it is possible to insert the positions of the reinforcement bars from the lines drawn in absolute coordinates, unlike the standard method, in which it is necessary to use relative coordinates in respect to the base elements, generating mesh dependence.

The steel profile was modeled by quadrilateral shell elements, named SHELL181 in ANSYS [9], with 4 nodes and 6 degrees of freedom per node (x, y, z translations and rotations), considering membrane and bending stiffnesses. Its formulation is based on the work of several authors, including Bathe and Dvorkin [11] and MacNeal and Harder [12], and uses Mindlin-Reissner's first-order shear-deformation theory. It is applicable to linear and nonlinear problems, including large deformations and rotations. For this reason, the formulation uses logarithmic strain and true stress measures rather than nominal engineering strain and stress. For small deformations, the difference between nominal and true values is negligible. The element can also contain several layers, and in the present work a single and centralized layer was used, with five integration points along the thickness.

The connectors were modeled by nonlinear spring elements, called COMBIN39 in ANSYS [9], acting in the longitudinal direction of the beam. Thus, the relative slip of the profile and slab nodes in this direction (u_x) are governed by points of the force versus slip curve of the element, whose data are obtained from push-out tests. When acting on a single degree of freedom per node, these elements should preferably be applied to coincident nodes [9]. In this work, however, they were applied to nodes spaced by half the thickness of the superior flange ($t_{fs}/2$), in function of the model geometry and the centralized positioning of the profile shell elements cross-section, as shown in Fig. 3. However, once this distance is very small, it can be assumed that these nodes are practically coincident. In the transverse and vertical directions, the coupling of the displacements u_y and u_z of these same nodes is performed. Thus, the COMBIN39 element acts only in the longitudinal direction of the beam, and compatibility equations are responsible for simulating the behavior of connectors in the other directions, as in the model proposed by Queiroz, Vellasco and Nethercot [13].

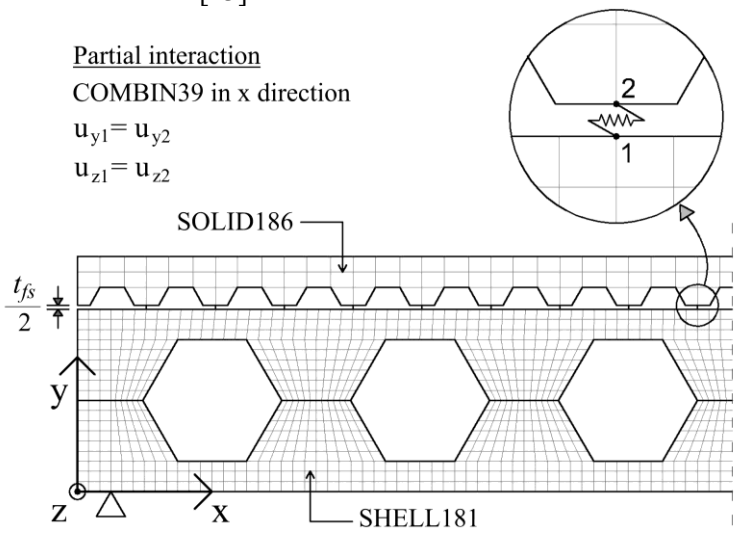

Figure 3. Connectors in the numerical model.

The steel-deck sheet was modeled by shell elements, assuming perfect interaction with the concrete slab. For this purpose, the lower slab faces were selected for the mesh generation, using the same nodes of the SOLID186 elements, which have 8 nodes on each face. For reasons of shape compatibility, an eight-node shell element was used, called SHELL281 in ANSYS [9], with 6 degrees of freedom per node (x, y, z translations and rotations).

Figure 4 highlights the elements cited in the developed numerical model.

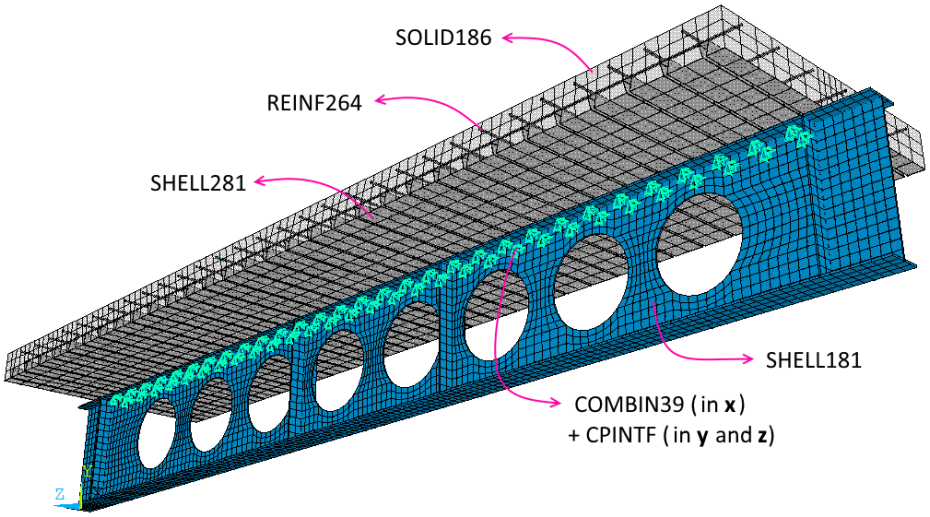

Figure 4. Element types in the numerical model.

2.2 Material models

For the simulation of the concrete behavior, two models have been used: (i) DP-Concrete and (ii) customized model via ANSYS usermat interface.

DP-Concrete is a native ANSYS model, available in the more recent versions of this software. A single Drucker-Prager surface does not represent the large differences in tensile and compressive behavior of concrete. Thus, the DP-Concrete model uses a Drucker-Prager plastification surface for compression, and a second surface, that may be Drucker-Prager or Rankine, for tension and tension-compression. Figure 5 illustrates the composition Drucker-Prager with Rankine, which was used in the present work, in the two-dimensional principal stress plane. The surfaces formulations are presented below, based on Chen [14] and ANSYS [9].

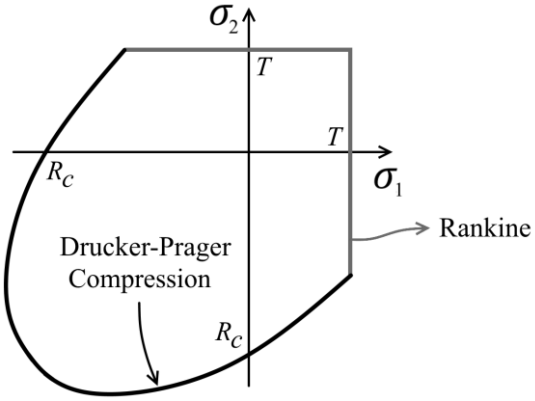

Figure 5. Combination DP-Rankine (adapted from [9]).

The Rankine surface in tension and tension-compression is defined by Eq. (1).

$$f_R = \sigma_m + \frac{2}{3}.\sigma_e.cos(\theta) - T.\Omega_t = 0. \tag{1}$$

$$\cos(3\theta) = \frac{3\sqrt{3}}{2}.\frac{J_3}{\sqrt{J_2^3}}. \tag{2}$$

Where $\sigma_m = I_1/3$ is the hydrostatic stress; I_1 is the first stress invariant; J_2 is the second deviatoric stress invariant; $\sigma_e = \sqrt{3J_2}$ is the von Mises stress; J_3 is the third deviatoric stress invariant; θ is the similarity angle, defined by Eq. (2); T is the uniaxial tensile strength of concrete; and Ω_t is the tension function of the adopted HSD model.

While the value of f_R is less than zero, the tensile and tensile-compressive behavior is admitted as linear elastic. When f_R equals zero, the plastic regime starts, in which the cracking can be simulated, approximately, through increments of plastic strain. In this step, the Rankine surface moves according to the function Ω_t of the adopted HSD model.

The Drucker-Prager surface under compression is defined by Eq. (3).

$$f_{DPc} = \frac{\sigma_e}{\sqrt{3}} + \beta_c . \sigma_m - \sigma_{Yc} . \Omega_c = 0. \tag{3}$$

Where β_c, σ_{Yc} are the constants calculated from material parameters and Ω_c is the compression function of the adopted HSD model.

While the value of f_{DPc} is less than zero, the behavior in compression is admitted as linear elastic. When f_{DPc} equals zero, the plastic regime starts: the Drucker Prager surface moves according to the function Ω_c of the adopted HSD model. As a general rule, unless concrete is accepted as perfectly elastoplastic (without the adoption of any HSD model), all available HSD models are divided into two sections in the compression behavior: (i) hardening, which governs surface expansion, until the maximum compressive stress is reached; and (ii) softening, which governs the shrinkage of the surface, initiating the crushing process, after reaching the maximum compressive stress.

The values of the constants β_c e σ_{Yc} are calculated by Eq. (4) and (5).

$$\beta_c = \frac{\sqrt{3}.(R_b - R_c)}{2.R_b - R_c}. \tag{4}$$

$$\sigma_{Yc} = \frac{R_b . R_c}{\sqrt{3}.(2.R_b - R_c)}. \tag{5}$$

Where R_c is the uniaxial compressive strength of concrete [kN/cm²] and R_b is the biaxial compressive strength of concrete [kN/cm²].

Depending on the HSD (hardening, softening and dilatation) model adopted, the functions Ω_c and Ω_t assume a certain format. Through these models, it is possible to simulate, approximately, the phenomena of cracking, in the tensile behavior, and crushing, in the compressive behavior, through increments of plastic strain related to hardening and softening rules. ANSYS offers four types of HSD models. In this work the model HSD Linear, shown in Fig. 6, was used.

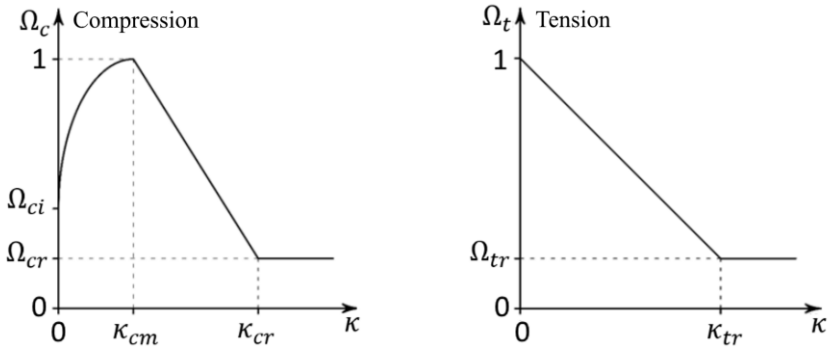

Figure 6. Linear HSD Model (adapted from [9]).

In Fig. 6, the graphs represent the values of the softening and hardening functions in compression and tension (Ω_c and Ω_t) in the ordinates, and the effective plastic strain (κ) in the abscissa. The other

parameters indicated in the graphs are input parameters, which can be adjusted to change the format of the functions. The softening laws in tension allow the effect of the contribution of concrete between cracks (known as tension stiffening phenomenon) to be considered. In the present work, the values of Ω_{ci} = 0.4; Ω_{cr} = 0.65; Ω_{tr} = 0.02 e κ_{tr} = 0.001 were adopted. On the other hand, the values of κ_{cm} and κ_{cr} were calibrated so that the total strains (elastic plus plastic) in compression were equal to 2‰ when the concrete reaches the maximum stress, and to 3.5‰ when the concrete reaches the residual stress.

It was also used, for purposes of results comparison, a customized model for concrete developed by Lazzari et al. [15], based on the Ottosen [16] criterion, through the ANSYS subroutine called usermat, which can be programmed to customize a material model [9]. The surface of Ottosen [16] is given by Eq. (6) and (7).

$$f(I_1, J_2, \cos(3\theta)) = \alpha.\frac{J_2}{f_{cm}^2} + \lambda.\frac{\sqrt{J_2}}{f_{cm}} + \beta.\frac{I_1}{f_{cm}} - 1 = 0. \tag{6}$$

$$\lambda = \begin{cases} c_1.\cos\left(\frac{1}{3}arccos(c_2.cos(3\theta))\right) & for \;\; cos(3\theta) \geq 0. \\ c_1.\cos\left(\frac{\pi}{3} - \frac{1}{3}arccos(-c_2.cos(3\theta))\right) & for \;\; cos(3\theta) \leq 0. \end{cases} \tag{7}$$

Where f_{cm} is the average compressive strength of concrete; $\alpha, \beta, c_1 \; and \; c_2$ are material parameters.

For the compressive behavior, the hardening law adopted is given by Eq. (8), illustrated in Fig.7(a), suggested by *fib2010* model code [17].

$$\frac{\sigma_c}{f_{cm}} = -\left(\frac{k.\eta - \eta^2}{1 + (k-2).\eta}\right). \tag{8}$$

Where σ_c is the compressive stress; ε_c is the compressive strain of concrete; ε_{c1} is the strain at the maximum compressive stress; $\varepsilon_{c,lim}$ is the ultimate compressive strain; E_{ci} is the initial tangent modulus of elasticity of concrete; E_{c1} is the secant modulus of elasticity of concrete; $k = E_{ci}/E_{c1}$ is the plastic number; and $\eta = \varepsilon_c/\varepsilon_{c1}$.

For the tensile behavior, a model of distributed cracks was adopted, considering the tension stiffening effect through the softening law shown in Fig. 7(b). Initially, the concrete is admitted as linear elastic until the tensile strength (f_{ctm}) is reached. After the cracking occurs, the softening is governed by a decreasing line that intersects the vertical axis in the value of $\alpha.f_{ctm}$ and the horizontal axis in the limit strain value (ε_{ctu}). In the present work, α=0.6 e ε_{ctu}=0.001 were adopted.

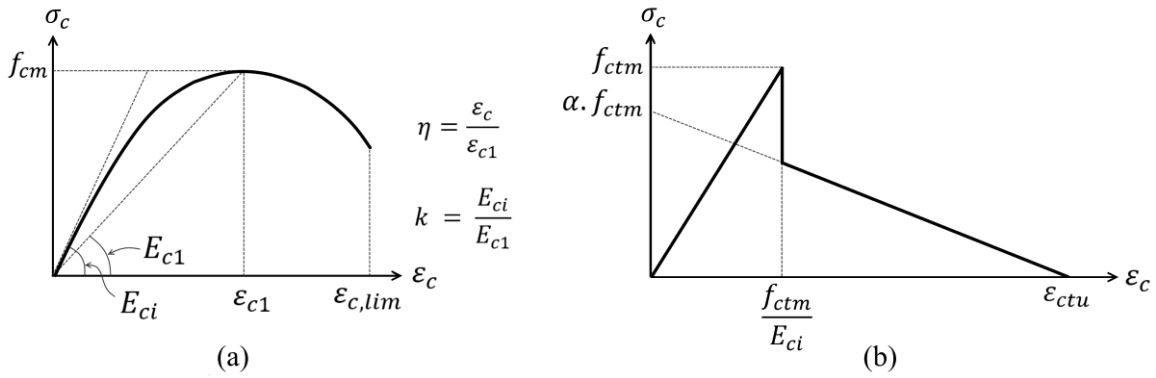

Figure 7. Constitutive laws for concrete in usermat model: (a) compression; (b) tension.

The profile steel was modeled by von Mises plastification criterion for yielding with isotropic hardening. As hardening law, the constitutive model proposed by Gattesco [18], shown in Fig. 8(a), was adopted. This model is divided into three stages of loading: (i) elastic-linear; (ii) yield plateau; (iii)

hardening governed by parabolic curve, given by Eq. (9). On the other hand, steels of the reinforcement bars and the steel deck sheet were simplified as perfectly elastoplastic, as shown in Fig. 8(b).

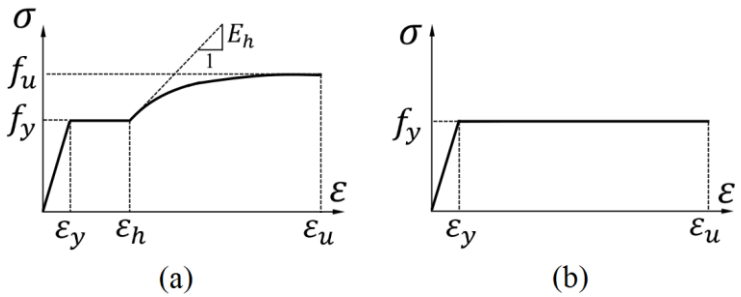

Figure 8. Constitutive laws: (a) profile steel; (b) reinforcement bars and steel-deck steels.

$$\sigma = f_y + E_h.(\varepsilon - \varepsilon_h).\left(1 - \frac{E_h.(\varepsilon - \varepsilon_h)}{4.(f_u - f_y)}\right). \tag{9}$$

Where f_y and f_u are the steel yielding and ultimate strengths, ε_y is the strain at steel yielding stress, ε_h is the strain at the initial hardening, ε_u is the strain at ultimate stress, E is the steel modulus of elasticity and e E_h is the tangent modulus of elasticity.

Unlike other materials, the steel properties of the connectors are not inserted into a material model itself, but rather through real constants of the COMBIN39 spring element. These real constants provide points for the force versus slip curve obtained experimentally via the push-out test. In order to standardize the model, the theoretical curve given by Eq. (10), as proposed by Ollgaard, Slutter and Fisher [19], adjustable to the push-out test data of stud bolts, was adopted.

$$Q = Q_{máx}.(1 - e^{-ms})^n. \tag{10}$$

Where Q is the shear force acting in the connector [kN]; $Q_{máx}$ is the maximum shear force resisted by the connector [kN]; s is the slip [mm]; e = 2,718 is the Euler number; and m e n are curve fitting parameters, in mm^{-1} and dimensionless, respectively.

2.3 Boundary Conditions

The developed model admits the beams as simply supported and uses the symmetry condition. Thus, the nodes at the first support, on the lower face of the beam, had the displacements in y and z restricted; and the nodes at the central cross-section of the beam had the displacements in x and the rotations around y and restricted, as shown in Fig. 9. The load was applied by imposing y-displacements on the nodes located at the respective points of application.

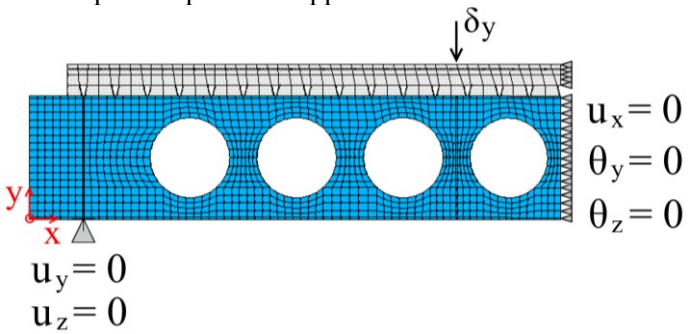

Figure 9. Boundary conditions.

2.4 Stages of the solution

The numerical problem was solved in four stages, aiming at the model's ability to simulate local instability effects in nonlinear analysis:

Stage 1*:* Solution of a base static analysis, by applying a unit load distributed among the same nodes as the final load.

Stage 2*:* Solution of an Eigen-Buckling analysis, by solving the problem of eigenvectors and eigenvalues, to determine buckling modes and load factors associated with the base static analysis.

Stage 3*:* Addition of geometric imperfections in the steel profile by updating the model geometry, based on the deformed buckling modes obtained, multiplied by weighting factors. In this work, the weighted combination of the first two modes was employed, each one with an amplitude of dg/600, dg being the height of the expanded profile. This amplitude value was suggested by Bake [20].

Stage 4*:* Final nonlinear analysis, by imposing y-displacements, divided into substeps. In this stage the Newton-Raphson method was used to solve the nonlinear problem.

3 Analyzed examples

Two beams, experimentally tested by Nadjai et al. [8], named A1 and B1, were modeled. The geometry of these beams is shown in Figs. 10 and 11. In both beams, a stud bolt connector per rib has been allocated, i.e. every 15 cm, with a diameter of 19 mm and a height of 120 mm. The concrete presented average compressive strength of 3.5 kN/cm², measured in test. A welded steel mesh with uniform spacing of 20 cm between bars with a diameter of 6 mm (A142 mesh) was used. The properties adopted for the materials in both numerical models are presented in Table 1. Some concrete properties, not provided by the authors, were calculated by the model code fib2010 [17] from the value of f_{cm}. It is noteworthy that, for the analysis with the DP-Concrete model, a reduced modulus was used, since the initial domain of the stress-strain curve is approximated by a linear function until the stress reaches the value of $0.4.f_{cm}$. For this purpose, the value of $0.9.E_{ci}$ was adopted in the two analyzed beams.

Beams A1 and B1 differ because of the geometry of the alveolar steel profile and the point of application of the loads, as shown in Figs. 10 and 11. The numerical models developed are shown in Figs. 12 and 13, with the symmetry condition. Table 2 indicates the number of elements used in each model.

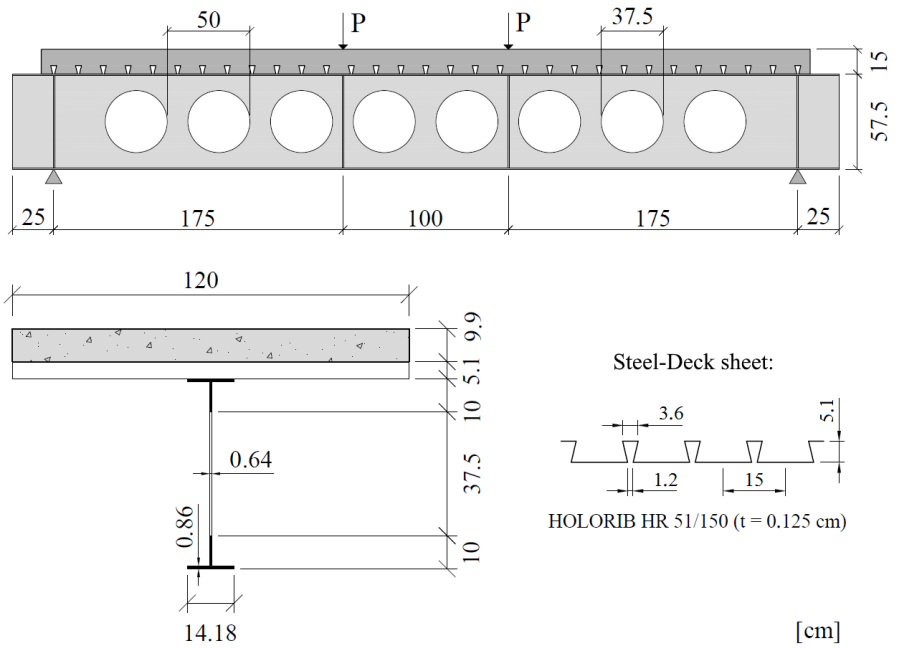

Figure 10. Geometry of beam A1 (adapted from [8]).

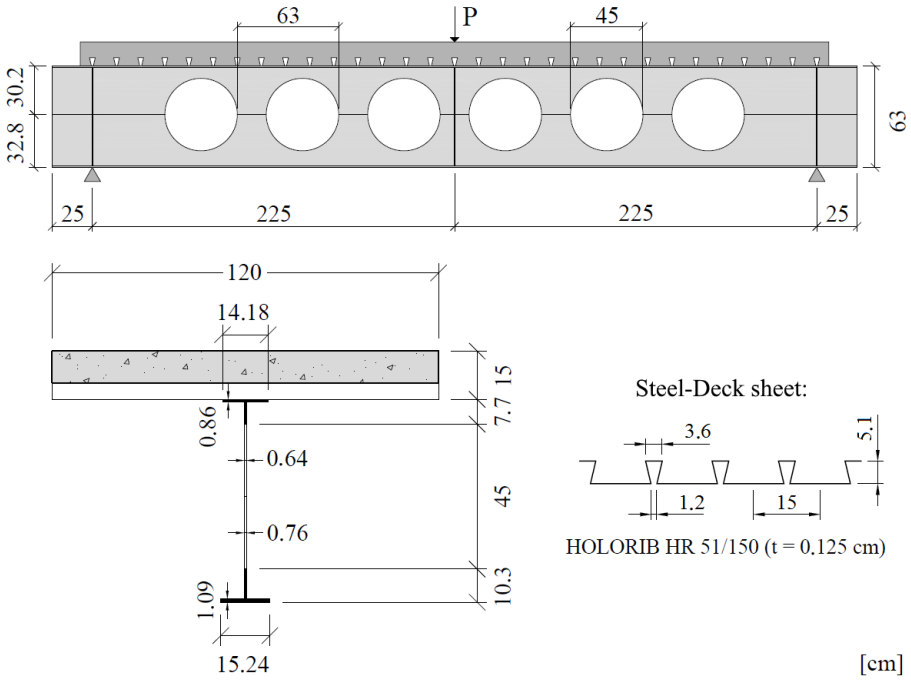

Figure 11. Geometry of beam B1 (adapted from [8]).

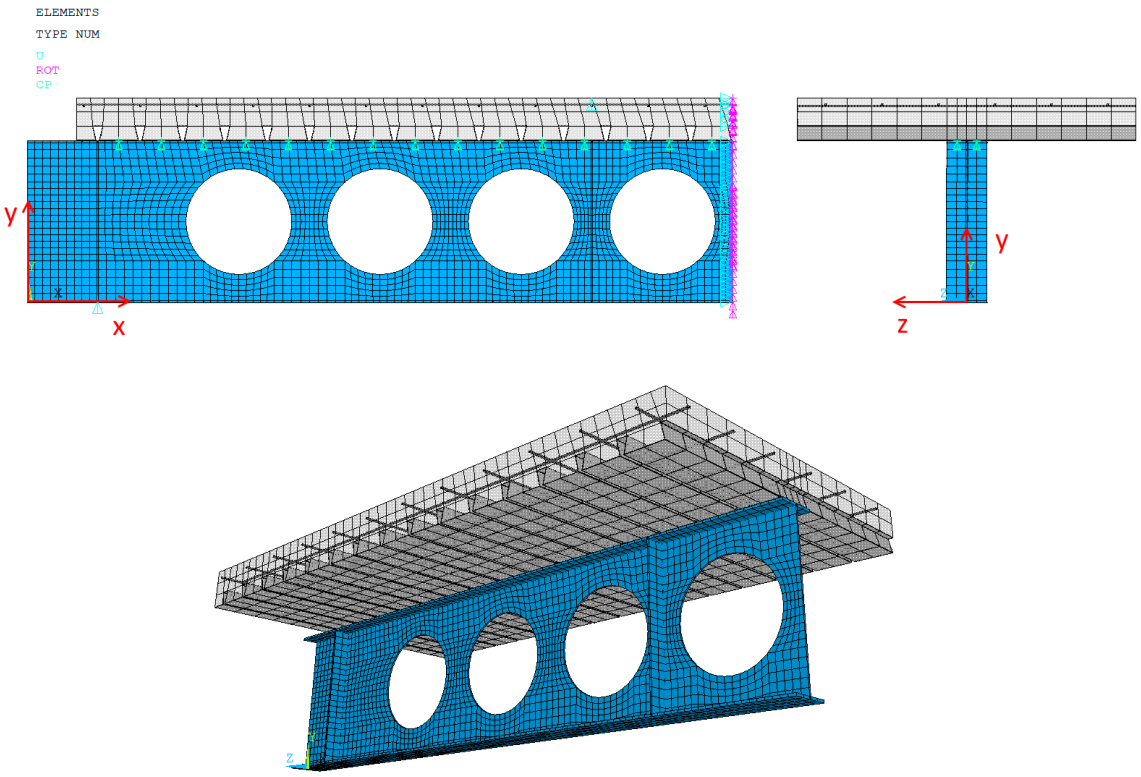

Figure 12. Numerical model of beam A1.

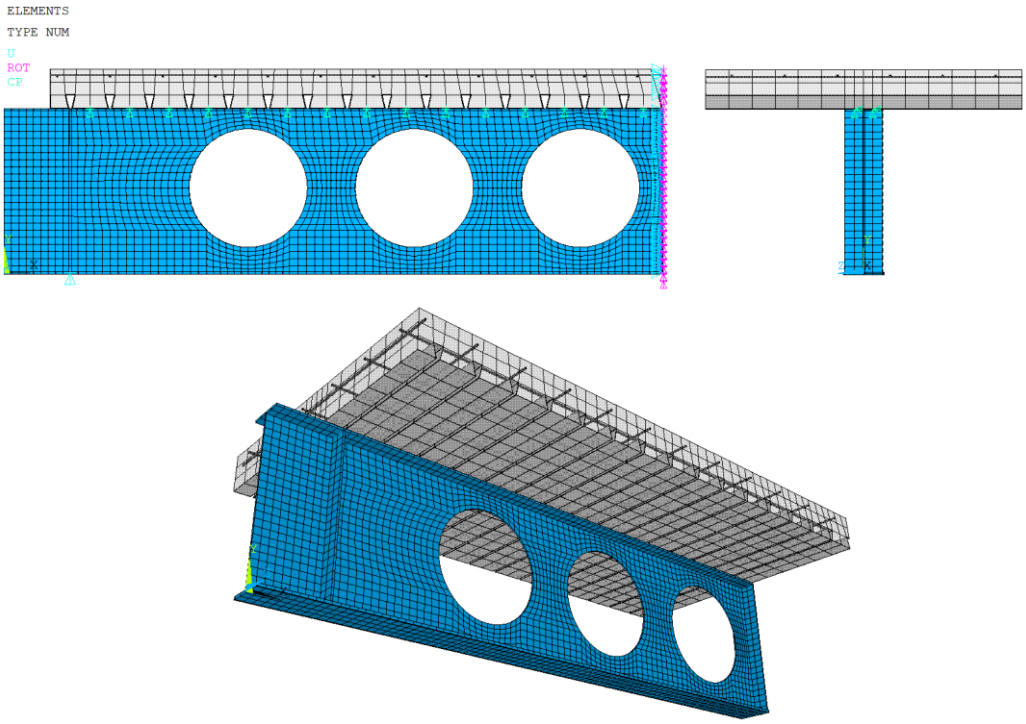

Figure 13. Numerical model of beam B1.

Table 1. Materials parameters adopted for the numerical models.

Material	Parameter	Value	Unit	Source
Profile Steel	E	20000	kN/cm²	Arbitrated, usual value
	f_y	31.2	kN/cm²	Bake [20]
	f_u	43.85	kN/cm²	
	$\varepsilon_h/\varepsilon_y$	7.5	-	Arbitrated
	E_h	400	kN/cm²	
Connectors	$Q_{máx}$	110	kN	Arbitrated based on the values adopted by Schmitz [22] for same diameter connectors
	m	1.3	1/mm	
	n	1	-	
Concrete	f_{cm}	3.5	kN/cm²	Nadjai *et al.* [8]
	E_{ci}	3264	kN/cm²	Calculated based on model code fib2010 [17]
	f_{ck}	2.7	kN/cm²	
	f_{ctm}	0.27	kN/cm²	
	f_{c2m}	4.08	kN/cm²	
Steel from Steel-Deck	E	21000	kN/cm²	Arbitrated, usual value
	f_y	32.7	kN/cm²	Nadjai *et al.* [8]
Reinforcement Steel	E	21000	kN/cm²	Arbitrated, usual value
	f_y	46	kN/cm²	Nadjai *et al.* [8]

Table 2. Number of elements in the numerical models.

Element type	Number of elements	
	Beam A1	Beam B1
SOLID186	2000	2000
SHELL181	2423	2629
SHELL281	1248	1248
COMBIN39	30	30
REINF264	402	402
Total	6103	6309

4 Results and discussion

Figures 14 and 15 display the obtained results by the present work, with DP-Concrete and usermat models, of the total load applied versus midspan deflection relationships for the beams A1 and B1, along the experimental results by Nadjai et al. [8] and numerical results by Bake [20] and Ferrari [21], who also analyzed these beams numerically.

In the experimental tests, both beams failed by buckling of the web post due to shear. Numerical models were able to capture this failure mode, as highlighted in Fig. 14 and 15, and illustrated by the z-displacements of beam A1 in Fig. 16, when u_y = 1.4 cm. The addition of geometric imperfections to the model through the combination of elastic buckling modes has proved to be an appropriate strategy to capture this mode of collapse.

Both numerical models of this work were able to capture the behavior of the analyzed beams with good precision, since their results showed a good correlation with the experimental results. Moreover, it is possible to notice that both models adopted for concrete – DP-Concrete and usermat – presented very similar results. Figure 17 shows the normal stresses in x on beam A1, when u_y = 1.0 cm, obtained by both models.

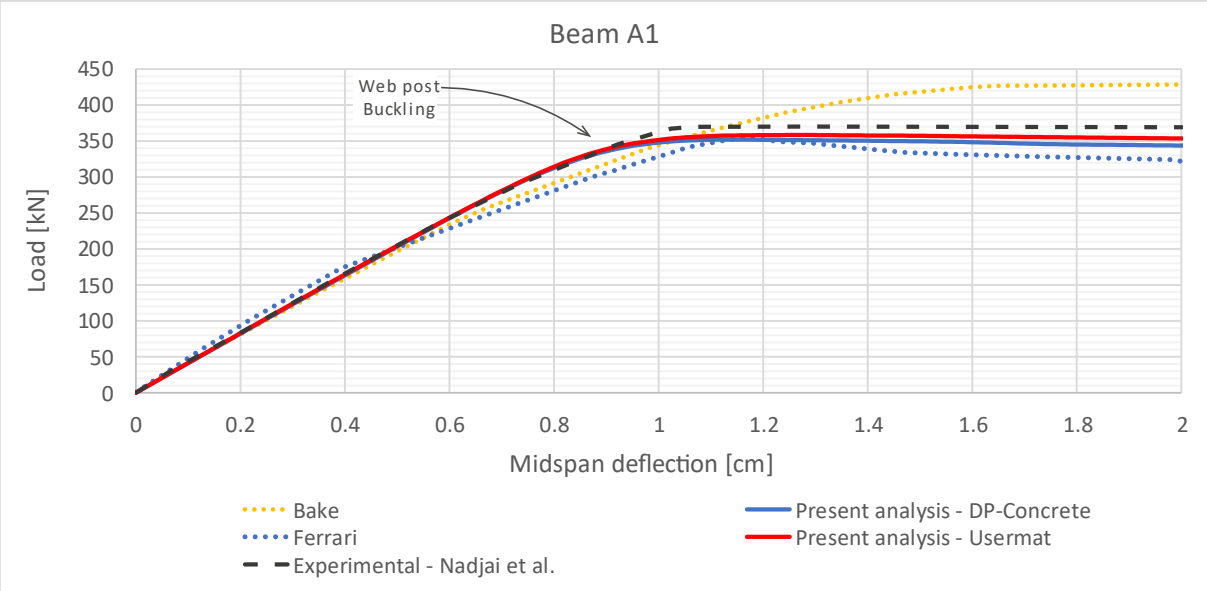

Figure 14. Load-deflection curve – Beam A1.

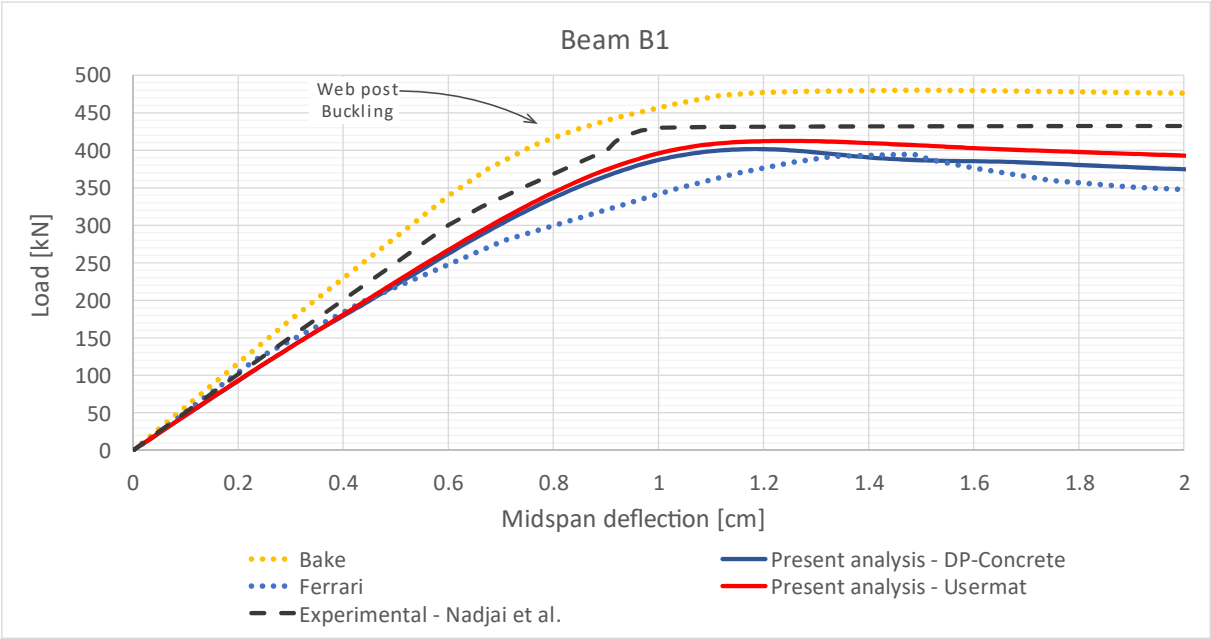

Figure 15. Load-deflection curve – Beam B1.

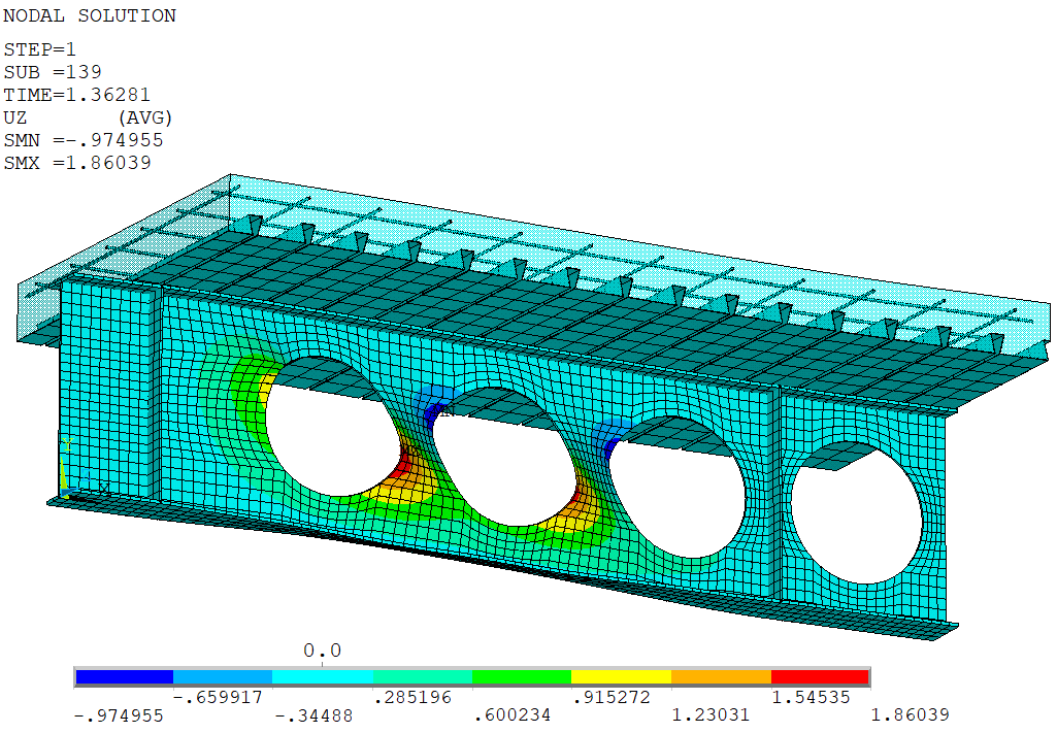

Figure 16. Beam A1: displacements in z when u_y=1.4 cm.

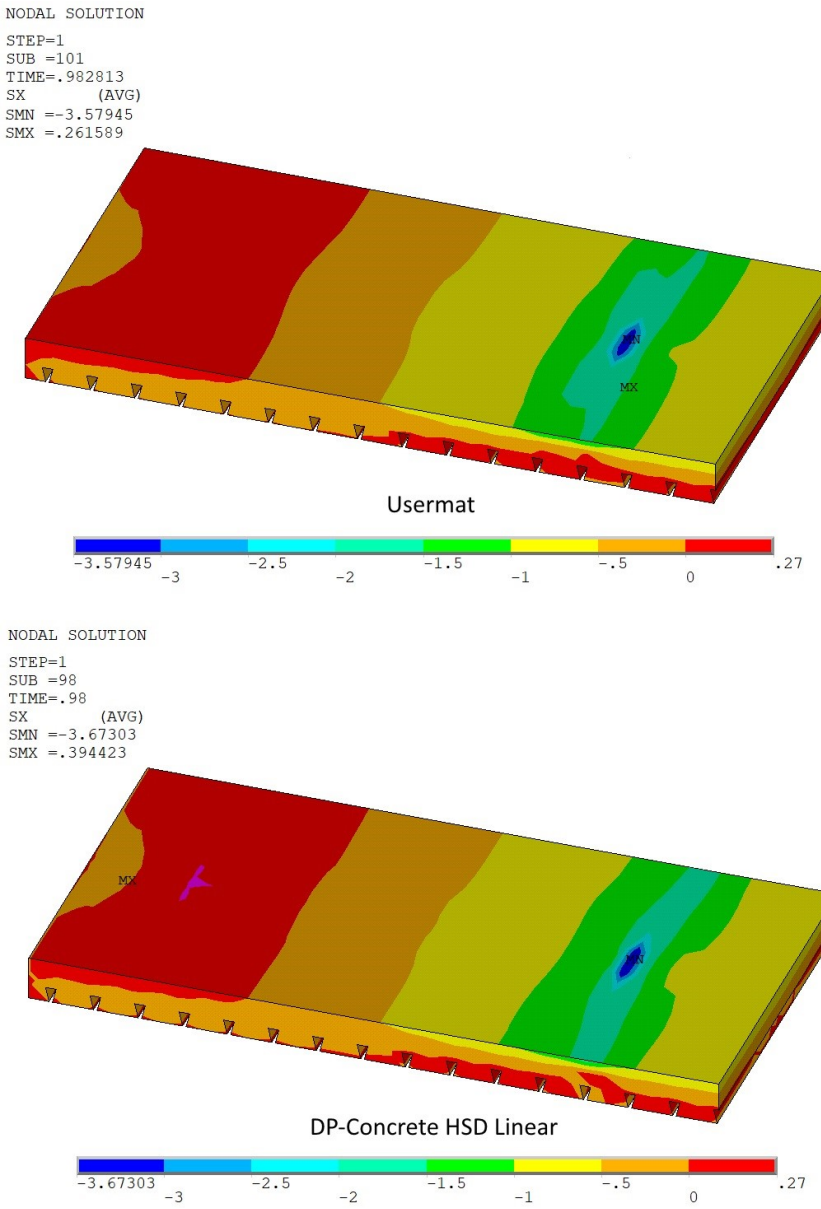

Figure 17. Beam A1: Comparison between the normal x-stresses obtained, when u_y=1.0 cm.

5 Conclusions

A finite element numerical model was developed in ANSYS software, version 19.2, for the simulation of composite alveolar beams, using two different material models for concrete. The obtained results with this model showed good correlation with the experimental results of two beams tested by Nadjai et al. [8] and with numerical results from previous works.

The models were able to capture the experimental collapse mode, that was buckling of the web post due to shear. For that, it was essential to add initial irregularities to the steel profile through the weighted combination of buckling modes, obtained from previous Eigen-Buckling analysis.

The two models adopted for concrete – DP-Concrete and Usermat – presented very similar results, which increases the reliability of the developed numerical model, as well as of each one of these material models.

Finally, it is concluded that the developed model was able to adequately simulate the behavior of the two analyzed beams. Further investigations should be performed to evaluate the model's ability to capture other modes of collapse.

Acknowledgements

The authors are grateful to CAPES and CNPq for their financial support for this research activity, and to CEMACOM/UFRGS for the infrastructure to carry out this work.

References

[1] T. I. Kotinda. Modelagem numérica de vigas mistas aço-concreto simplesmente apoiadas: ênfase ao estudo interface laje-viga. Master dissertation, Universidade de São Paulo, 2006.
[2] J. Nie, Y. Xiao and L. Chen. Experimental studies on shear strength of steel-concrete composite beams. *Journal of Structural Engineering*, v. 130, n. 8, pp. 1207-1213, 2004.
[3] A. B. Gonçalves. Modelo analítico para dimensionamento de vigas alveolares mistas de aço e concreto. Master dissertation, Universidade Federal de Viçosa, 2015.
[4] R. N. Brinkhus. Análise de vigas casteladas e vigas casteladas mistas. Master dissertation, Universidade Federal do Rio Grande do Sul, Porto Alegre, 2015.
[5] A. Badke-Neto, A. F. G. Calenzani and W. G. Ferreira. Estudo de metodologias para o dimensionamento de vigas mistas de aço e concreto com perfil celular. *Revista Ibracon de Estruturas e Materiais, São Paulo*, v. 8, n. 6, pp. 844-859, 2015.
[6] D. Kerdal and D. A. Nethercot. Failure modes for castellated beams. *Journal of Constructional Steel Research*, v. 4, n. 4, pp. 295-315, 1984.
[7] Constructalia. ArcelorMittal Global R&D Centre Spain: a showcase of the company's product range. Available at https://constructalia.arcelormittal.com/en. Accessed in July 2019.
[8] A. Nadjai, O. Vassart, F. Ali, D. Talamona, A. Allam and M. Hawes. Performance of cellular composite floor beams at elevated temperatures. *Fire Safety Journal*, v. 42, n. 6-7, pp. 489-497, 2007.
[9] ANSYS Inc. ANSYS help system: version 19.2. Canonsburg, 2018.
[10] O. C. Zienkiewicz. *The Finite Element Method*. McGraw-Hill Company, 1977.
[11] K. J. Bathe and E. N. Dvorkin. A formulation of general shell elements – the use of mixed interpolation of tensorial components. *International Journal for Numerical Methods in Engineering*, v. 22, pp. 697-722, 1986.
[12] R. H. MacNeal and R. L. Harder. A refined four-noded membrane element with rotational degrees of freedom. *Computers & Strucutures*, v. 28, n. 1, pp. 75-84, 1988.
[13] F. D. Queiroz, P. C. G. S. Vellasco and D. A. Nethercot. Finite element modelling of composite beams with full and partial shear connection. *Journal of Constructional Steel Research*, v. 63, n. 4, pp. 505–521, 2007.
[14] W. F. Chen. *Plasticity in reinforced concrete*. McGraw-Hill, 1982.
[15] P. M. Lazzari, A. Campos Filho, B. M. Lazzari, A. R. Pacheco and R. R. S. Gomes. Numerical simulation of the constructive steps of a cable-stayed bridge using ANSYS. *Structural Engineering and Mechanics*, v. 69, n. 3, pp. 269–281, 2019.
[16] N. S. A. Ottosen. Failure criterion for concrete. *Journal of the Engineering Mechanics Division ASCE*, v. 103, pp. 527–535, 1977.
[17] Féderation Internationale du Béton. *Model code fib2010*. Bulletin n. 65. Lausanne, 2012.
[18] N. Gattesco. Analytical modeling of nonlinear behavior of composite beams with deformable connection. *Journal of Constructional Steel Research*, v. 52, pp. 192–218, 1999.
[19] J. G. Ollgaard, R. G. Slutter and J. W. Fisher. Shear strength of stud connectors in lightweight and normal weight concrete. *AISC Engineering Journal*, New York, v. 10, n. 71, pp. 55-64, 1971.
[20] S. Bake. Behaviour of cellular beams and cellular composite floors at ambient and elevated temperatures. PhD thesis, University of Manchester, 2010.
[21] G. A. Ferrari. Simulação numérica do comportamento estrutural de vigas alveolares mistas de aço e concreto. Master dissertation, Universidade Federal de Viçosa, 2013.
[22] R. J. Schmitz. Estrutura mista aço-concreto: análise de ponte composta por vigas de alma cheia. Master dissertation, Universidade Federal do Rio Grande do Sul, Porto Alegre, 2017.